Bending and Warpage of Elastic Plates

Harrison G. Wood

Thesis submitted to the Faculty of the
Virginia Polytechnic Institute and State University
in partial fulfillment of the requirements for the degree of

Master of Science
in
Engineering Mechanics

James Hanna, Chair
Romesh C Batra
Scott W Case

May 9, 2019
Blacksburg, Virginia

Keywords: Plate Theory, Bending, Swelling, Elastic Energy

Bending and Warpage of Elastic Plates

Harrison G. Wood

Abstract

This thesis presents two studies on elastic plates. In the first study, we discuss the choice of elastic energies for thin plates and shells, an unsettled issue with consequences for much recent modeling of soft matter. Through consideration of simple deformations of a thin body in the plane, we demonstrate that four bulk isotropic quadratic elastic theories have fundamentally different predictions with regard to bending behavior. At finite thickness, these qualitative effects persist near the limit of mid-surface isometry, and not all theories predict an isometric ground state. We discuss how certain kinematic measures that arose in early studies of rod mechanics lead to coherent definitions of stretching and bending, and promote the adoption of these quantities in the development of a covariant theory based on stretches rather than metrics.

In the second work, the effects of in-plane swelling gradients on thin, anisotropic plates are investigated. We study systems with a separation of scales between bending energy terms. Warped equilibrium shapes are described by two parameters controlling the spatial "rolling up" and twisting of the surface. Shapes within this two-parameter space are explored, and it is shown that shapes will either be axisymmetric or twisted depending on swelling function parameters and material anisotropy. In some axisymmetric shapes, pitchfork bifurcations to twisted solutions are observed by varying these parameters. We also show that a familiar soft mode of the catenoid to helicoid transformation of an isotropic material no longer exists with material anisotropy.

Bending and Warpage of Elastic Plates

Harrison G. Wood

General Audience Abstract

This thesis presents two studies on the subject of thin, elastic bodies, otherwise known as plates. Plate theory has important applications in many areas of life, ranging from the design and construction of civil structures to the mechanics of wrinkling sheets. In the first work, we discuss how different elastic plate theories have qualitatively different predictions on how a plate will behave when bent. We discuss the different physical implications of each model, and relate our findings to previous studies. Additionally, we promote the use of certain technical measures in the study of plates corresponding to the most coherent definitions of bending and stretching.

In the second work, we study the effects of in-plane swelling gradients on elastic plates whose material stiffnesses vary with direction. Inspired by wood panels that warp when exposed to moisture, we model elastic plates exposed to various swelling patterns and determine the resulting warped shapes. We find that some shapes are axisymmetric, while others prefer to twist when exposed to moisture-induced swelling. By varying certain parameters of the swelling functions, or by increasing the material fiber stiffness, we also find a qualitative change in shape from an axisymmetric to a twisted surface.

This work was partially funded by the Wood-Based Composites Center, a National Science Foundation Industry/University Cooperative Research Center. (Award 1624536-IIP)

Contents

Chapter 1

Introduction

The material presented in this thesis focuses on the study of elastic plates, models of their energies, and their deformations as a result of swelling gradients. This includes comparing various isotropic energy models and discussing their physical implications for thin plates, and studying the effects of in-plane swelling gradients on resulting shapes of anisotropic plates.

Plate theory has a broad range of application in science, engineering, and industry, and can provide insight into certain physical systems. Industry applications include laminated composite materials for the aerospace, wood, and civil structures industries, as well the design and implementation of printable and shape-programmable materials. From a more academic standpoint, the study of plates can provide new information on the behavior of common phenomena such as the wrinkling of sheets, tearing plastic trash bags, and the complex shapes of leaves.

The content of this thesis is broken up into two independent manuscripts that appear as separate chapters. In Chapter 2, four separate elastic theories and the different predictions they have on the bending behavior of a thin plate are studied. By considering two simple deformations, it is shown that these differences persist near the limit of a mid-surface isometry. The advantages and disadvantages of each model are discussed, and the promotion of certain definitions of stretching and bending in the context of plates and rods is made.

In Chapter 3, the effects of in-plane swelling gradients on the warped shapes of anisotropic plates are studied. Inspired by warping in engineered wood products that are exposed to moisture, and the lack of understanding of swelling in anisotropic materials, a reduced two-dimensional elastic energy model is used to determine equilibrium shapes for a given swelling function within a class of isometric surfaces. Shapes are found to be either axisymmetric or twisted, with some swelling functions resulting in surface shapes that can bifurcate to a twisted configuration by varying material or swelling patterns.

Chapter 2

Contrasting bending energies from bulk elastic theories

The contents of this chapter have appeared almost as-is in *Soft Matter*, volume 15, pages 2411-2417, 2019. The published article can be found at: `https://pubs.rsc.org/en/content/articlelanding/2019/sm/c8sm02297f#!divAbstract`.

Attribution

The work presented in this chapter was done in collaboration with J. A. Hanna, who contributed to the inception and development of the main ideas of this work.

Abstract

The choice of elastic energies for thin plates and shells is an unsettled issue with consequences for much recent modeling of soft matter. Through consideration of simple deformations of a thin body in the plane, we demonstrate that four bulk isotropic quadratic elastic theories have fundamentally different predictions with regard to bending behavior. At finite thickness, these qualitative effects persist near the limit of mid-surface isometry, and not all theories predict an isometric ground state. We discuss how certain kinematic measures that arose in early studies of rod mechanics lead to coherent definitions of stretching and bending, and promote the adoption of these quantities in the development of a covariant theory based on stretches rather than metrics.

2.1 Introduction

Much recent work in soft matter mechanics has explored the interplay of stretching and bending elasticity in incompatible plates and shells composed of isotropic gels or elastomers, or nematic solids [1, 2, 3, 4, 5]. This subject has inspired, among other things, fundamental questions about embeddings [6, 7, 8], design principles for shape-programmable materials [9, 10, 11, 12], and insight into the complex shapes of leaves and torn plastic trash bags [13, 14].

A work that has been particularly influential on the modeling efforts of several other groups in this community has been that of Efrati and co-workers [1], who introduced a formalism for isotropic incompatible elasticity of plates. This work chose a particular form of elastic energy, quadratic in invariants of Green strain. Issues have been raised with this strain energy [15, 16] that, while not detracting from the valuable conceptual framework developed in [1], have important consequences for any attempts to apply this theory to experiments or use it as a basis for building extended theories.

This note seeks to formalize, flesh out, and amplify a point raised by one of the present authors in a broader paper on plate elasticity [16], namely that constitutive choices of elastic energy that lead to higher-order effects in the bulk actually have significant *qualitative* effects on derived bending energies, even near the limit of vanishing strains. This is related to ambiguities in the choice of fundamental quantities for "small-strain" expansions. Such expansions, which are a standard approach in physics, are atypical in the continuum mechanics field, where it is also known that different simple constitutive choices for finite strain measures can have important consequences at moderate to large strains [17, 18].

In the context of two basic deformations of a two-dimensional, compatible plate or flat beam, we compare four isotropic "quadratic" elastic energies and their reduced one-dimensional forms within the Kirchhoff-Love framework. Of these, only one is quadratic in stretch (the ratio of present length to reference length) and leads to a bending energy quadratic in a simple kinematic bending variable favored in some direct theories of rods. The other bending energies are not only more complicated but lead to qualitatively different predictions for the behavior of the plate. This very simple calculation allows us to illustrate our point while sidestepping the development of a more general theory featuring shearability, the geometry of a two-dimensional surface, or other complexities. Yet our findings from this restricted example should be widely applicable. Additionally, we hope that the notational format we introduce here for Biot strains and similar tensors may prove useful to the soft matter community in developing new theories.

While much has been written on the contrasting limits of small bending and zero stretching in plates and shells, problems in which both stretching and bending are important are less well understood [19], despite being induced by common loading conditions. For example, pulling and rotating the ends of a sheet requires simultaneous changes in mid-surface lengths and curvatures, as does inflation of a closed vessel under internal pressure. Even the crumpling

regime, in which most of a sheet is approximately isometrically deformed, features significant stretching and bending condensation in "defects" whose fundamental structure is still a mystery [20]. Experiments, both tabletop and microscopic, in soft matter are often performed on moderately thin structures of the type found in engineering applications, where separation of scales is modest.

All of this is to say that bending energy is important, and so it would be a good idea to work with the right one. The appropriateness of a given energy could be determined by a connection with experimental observations or, if one seeks to predict material-agnostic behaviors, by the simplicity of an otherwise reasonable choice. However, convenient choices for expressing bulk elasticity as an expansion based on position derivatives differ from those that simplify direct models of low-dimensional bodies [16].

Consider the following question, based on whatever intuition you may have for common elastic materials. Take a thin plate of such a material and bend it into a cylindrical ring, and fuse the ends so that the midplane is unstretched. Will the ring:

1. Expand to relieve bending and pay some stretching cost (the prediction of an energy quadratic in Almansi or Swainger strains),
2. Stay the same radius (Biot strain),
3. Contract to a smaller radius to relieve bending and pay some stretching (compressive) cost (Green strain)?

It is likely a surprise to many soft matter researchers that they have been working with option 3 for quite a few years. Perhaps less intuitively obvious is that option 1 is equally undesirable from the point of view of simple direct theories of beams and plates. A related question is, how do we wish to define a measure of bending, and by extension a bending energy and the concept of a pure stretching deformation, for a thin structure? One possible answer is that we'd like a bulk energy density quadratic in some measure of strain, a reduced energy density quadratic in the corresponding derived measure of bending, and a linear relationship between this bending measure and the internal moment. These simultaneous requirements are not trivial to fulfill, and correspond to option 2.

In this note, we consider energies quartic or quadratic in stretch or inverse stretch, built from the quadratic invariants of four types of strain. All of these invariants are approximately identical for stretches near unity. The energies can be informally thought of in the following way,

> Green: quartic, reference
> Biot: quadratic, reference
> Almansi: inverse quartic, present
> Swainger: inverse quadratic, present

Using convected material coordinates, the *covariant* components of Green strain in the co-

ordinate reference basis and those of Almansi strain in the present basis are simply (one half of) the familiar metric differences [21], quadratic in stretch. Invariants of these two tensors are formed by raising indices and contracting with the components of the reference or present metrics, respectively. The Almansi form leads to natural geometric quantities such as curvatures of deformed plates and membranes. The *mixed* components of Biot strain in the reference basis are linear in stretch, and those of Swainger in the present basis are inverse linear. Another way to express this is that Biot is the finite elastic version of the naive measure given by change in length over reference length, while Swainger is change in length over present length. We will see that to the usual quadratic order in bending terms, the two "present" energies, Almansi and Swainger, give the same bending energy, qualitatively distinct from those arising from Green or Biot.

Biot and similar measures have arisen explicitly or implicitly in both soft matter physics and continuum mechanical works, either as a natural consequence of bead-spring models of molecular mesostructures [22, 23], from a desire to obtain simple constitutive relations between moment and kinematic variables [15, 24], or from a recognition that a reduction process will generate certain direct theories of rods [25, 26, 27, 28]. Such direct theories [29, 30, 31] for low-dimensional objects are constructed from a convenient choice of kinematic variables without consideration of whether they inherit their form from a bulk elastic theory.

After defining strains and other quantities in Section 2.2, we derive reduced energies for a restricted geometry in Section 2.3, and examine these for two simple operations in Section 2.4, namely the expansion of a closed circular ring, and the extension of a circular arc at fixed radius. We finish with some comments in Section 2.5.

2.2 Geometry

Consider a body in the plane, with uniform thickness $t \ll 1$, parameterized by material coordinates x and z in the axial and thickness directions, respectively. Its present position is $\mathbf{r}(x, z)$ and that of its mid-line is $\mathbf{x}(x) = \mathbf{r}(x, 0)$. These two- and one-dimensional objects have natural coordinate bases $\mathbf{g}_i = \partial_i \mathbf{r}$ and $\mathbf{a}_x = \partial_x \mathbf{x} = \mathbf{g}_x(x, 0)$, respectively. The mid-line has a unit normal $\hat{\mathbf{n}}$. The body also has corresponding reference quantities $\mathbf{R}$, $\mathbf{X}$, $\mathbf{G}_i$, $\mathbf{A}_x$, and $\hat{\mathbf{N}}$. For simplicity we take x to be the reference arc length, so that $\mathbf{A}_x$ is a unit vector. Reciprocal bases of inverse tangents are defined such that $\mathbf{g}^i \cdot \mathbf{g}_j = \delta^i_j$ and $\mathbf{G}^I \cdot \mathbf{G}_j = \delta^I_j$, with the definitions of $\mathbf{a}^x$ and $\mathbf{A}^X$ following in the obvious way. Capitalization on upper indices is simply a reminder that such indices appearing on reference objects are not raised with the present inverse metric; implied summation ignores case [16]. Note that x and z or X and Z will always serve as specific material indices and not free or summable indices. Metric and inverse metric components can be defined using the tangent vectors and their inverses, but we will not need them. The deformed mid-line is conveniently described using a stretch $\Lambda(x)$ and a tangential angle $\theta(x)$, so that the tangent and normal have Cartesian representations

$\mathbf{a}_x = \partial_x \mathbf{x} = \Lambda \begin{pmatrix} \cos\theta \\ \sin\theta \end{pmatrix}$ and $\hat{\mathbf{n}} = \begin{pmatrix} -\sin\theta \\ \cos\theta \end{pmatrix}$. Figure 2.1 is a schematic of the reference and present configurations.

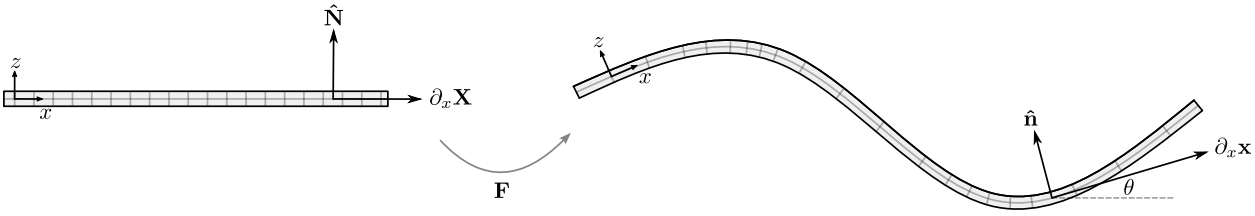

Figure 2.1: Reference and present configurations of a thin body in the plane.

The deformation gradient $\mathbf{F} = \mathbf{g}_i \mathbf{G}^I$ maps line elements from reference to present configurations, $\mathbf{F} \cdot d\mathbf{R} = d\mathbf{r}$. It will be used along with its transpose $\mathbf{F}^T = \mathbf{G}^I \mathbf{g}_i$ to construct four symmetric tensors. The right and left Cauchy-Green deformation tensors are $\mathbf{C} = \mathbf{F}^T \cdot \mathbf{F}$ and $\mathbf{B} = \mathbf{F} \cdot \mathbf{F}^T$. The right and left stretch tensors are defined by the decompositions $\mathbf{F} = \mathbf{Q} \cdot \mathbf{U} = \mathbf{V} \cdot \mathbf{Q}$, where $\mathbf{Q}$ is a rotation tensor. The four strains of interest involve $\mathbf{C}$, $\mathbf{U}$, the inverses $\mathbf{B}^{-1}$ and $\mathbf{V}^{-1}$, and the identity $\mathbf{I}$, where the inverse of a symmetric tensor $\mathbf{T}$ is defined such that $\mathbf{T} \cdot \mathbf{T}^{-\mathbf{1}} = \mathbf{T}^{-\mathbf{1}} \cdot \mathbf{T} = \mathbf{I}$.

For exemplary — not endorsement — purposes, we consider the idealized constrained kinematics of the Kirchhoff-Love assumptions and associated standard but non-rigorous procedures for deriving a reduced energy. The first Kirchhoff-Love assumption tells us that the x and z directions correspond to principal stretches $\Lambda_x(x,z)$ and $\Lambda_z(x,z)$. We will write things in somewhat non-traditional format using mixed reference or present bases in principal directions. As with the non-coordinate orthonormal principal direction bases commonly used in continuum mechanics [32], the invariants can be read off easily from these mixed components, but we believe this representation will be more amenable to future theoretical generalizations in convected coordinates.[1]

Thus, in the restricted situation we are concerned with, the relevant deformation tensors may be written as

$$\text{right Cauchy-Green} \quad \mathbf{C} = \Lambda_x^2 \mathbf{G}_x \mathbf{G}^X + \Lambda_z^2 \mathbf{G}_z \mathbf{G}^Z, \tag{2.1}$$

$$\text{inverse left Cauchy-Green} \quad \mathbf{B}^{-1} = (1/\Lambda_x^2) \mathbf{g}_x \mathbf{g}^x + (1/\Lambda_z^2) \mathbf{g}_z \mathbf{g}^z, \tag{2.2}$$

$$\text{right stretch} \quad \mathbf{U} = \Lambda_x \mathbf{G}_x \mathbf{G}^X + \Lambda_z \mathbf{G}_z \mathbf{G}^Z, \tag{2.3}$$

$$\text{inverse left stretch} \quad \mathbf{V}^{-1} = (1/\Lambda_x) \mathbf{g}_x \mathbf{g}^x + (1/\Lambda_z) \mathbf{g}_z \mathbf{g}^z, \tag{2.4}$$

[1] We note one disadvantage of this asymmetric representation of symmetric tensors. When used in concert with our adoption above of the traditional transpose notation for the deformation gradient (the latter is unfortunately entrenched in continuum mechanics, and serves to indicate which tensor legs the inner product refers to), one may get the mistaken impression that it might make sense to write transposes of these symmetric tensors. To be consistent, one should either replace the transpose notation, or symmetrize the bases in expressions such as (2.1-2.8). We emphasize that these expressions are not general, but work for our restricted situation.

and the corresponding strain tensors as

$$\begin{aligned}
\text{Green} \quad \tfrac{1}{2}(\mathbf{C}-\mathbf{I}) &= \tfrac{1}{2}\left(\Lambda_x^2-1\right)\mathbf{G}_x\mathbf{G}^X + \tfrac{1}{2}(\Lambda_z^2-1)\mathbf{G}_z\mathbf{G}^Z, && (2.5)\\
\text{Almansi} \quad \tfrac{1}{2}(\mathbf{I}-\mathbf{B}^{-1}) &= \tfrac{1}{2}\left(1-1/\Lambda_x^2\right)\mathbf{g}_x\mathbf{g}^x + \tfrac{1}{2}\left(1-1/\Lambda_z^2\right)\mathbf{g}_z\mathbf{g}^z, && (2.6)\\
\text{Biot} \quad \mathbf{U}-\mathbf{I} &= (\Lambda_x-1)\,\mathbf{G}_x\mathbf{G}^X + (\Lambda_z-1)\mathbf{G}_z\mathbf{G}^Z, && (2.7)\\
\text{Swainger} \quad \mathbf{I}-\mathbf{V}^{-1} &= (1-1/\Lambda_x)\,\mathbf{g}_x\mathbf{g}^x + (1-1/\Lambda_z)\,\mathbf{g}_z\mathbf{g}^z. && (2.8)
\end{aligned}$$

The Green and Almansi tensors will be more familiar to physicists as $\gamma_{ij}\mathbf{G}^I\mathbf{G}^J$ and $\gamma_{ij}\mathbf{g}^i\mathbf{g}^j$, using the metric differences $2\gamma_{ij} = \mathbf{g}_i\cdot\mathbf{g}_j - \mathbf{G}_i\cdot\mathbf{G}_j$, a form that holds for more general deformations.

A two-dimensional, isotropic, quadratic energy in terms of a nonspecific strain tensor $\boldsymbol{\epsilon}(\mathbf{r})$ will take the form

$$\int d\bar{A}\left[c_1\left(\mathrm{Tr}(\boldsymbol{\epsilon})\right)^2 + c_2\mathrm{Tr}\left(\boldsymbol{\epsilon}^2\right)\right], \tag{2.9}$$

where $d\bar{A} = 1dxdz$ is the simple reference volume measure and the c_i are moduli. The first Kirchhoff-Love assumption allows for determination of the transverse strain as proportional to the axial strain [1], $\epsilon^z{}_z = f(c_1,c_2)\epsilon^x{}_x$, and thus rewriting of the energy

$$\int dx\,\mathcal{E} = \int dx \int_{-t/2}^{t/2} dz\,\tilde{Y}\left(\epsilon^x{}_x\right)^2, \tag{2.10}$$

with some suitably defined modulus $\tilde{Y}$. After this, the second Kirchhoff-Love assumption can be invoked, setting the geometry of the present configuration as $\mathbf{r}(x,z) = \mathbf{x}(x) + z\hat{\mathbf{n}}(x)$ and allowing us to express the axial stretch $\Lambda_x(x,z)$ in terms of the mid-line stretch $\Lambda(x) = \Lambda_x(x,0)$ and angle $\theta(x)$ [28],

$$\Lambda_x(x,z) = \Lambda(x) - z\partial_x\theta, \tag{2.11}$$

so that we may integrate to explicitly obtain the density $\mathcal{E}$.

2.3 Four quadratic energies

We may now evaluate the forms of the energy density $\mathcal{E}$ from (2.10) that take as input the axial component of the four strains (2.5-2.8) containing the bulk axial stretch (2.11). For each density, this will result in quadratic terms involving one of the four corresponding mid-line strains $\varepsilon(\mathbf{x})$, namely

$$\begin{aligned}
\text{Green} \quad \varepsilon_{\mathrm{G}} &= \tfrac{1}{2}\left(\Lambda^2-1\right), && (2.12)\\
\text{Almansi} \quad \varepsilon_{\mathrm{A}} &= \tfrac{1}{2}\left(1-1/\Lambda^2\right), && (2.13)\\
\text{Biot} \quad \varepsilon_{\mathrm{B}} &= \Lambda-1, && (2.14)\\
\text{Swainger} \quad \varepsilon_{\mathrm{S}} &= 1-1/\Lambda, && (2.15)
\end{aligned}$$

and one of three bending measures,

1. Almansi or Swainger: The present arc length derivative of the tangential angle, which generates the invariant (Frenet) curvature $\partial_s\theta = \partial_x\theta/\Lambda$. In the Almansi context, this can be thought of as applying the inverse present metric to the covariant component of the curvature tensor, $(\mathbf{a}^x \cdot \mathbf{a}^x)\, b_{xx}$, where $b_{xx} = \partial_x \mathbf{a}_x \cdot \hat{\mathbf{n}} = \Lambda\partial_x\theta$.
2. Biot: The material derivative of the tangential angle $\partial_x\theta$,
3. Green: $\Lambda\partial_x\theta$, which can be thought of as obtained by applying the trivial inverse reference metric $\mathbf{A}^X \cdot \mathbf{A}^X$ to b_{xx}, viewed now as a component of some unnamed tensor.

While the four mid-line strains all linearize to $\Lambda - 1$ when Λ is close to unity, the three bending measures have qualitatively different forms. They are either inversely linearly dependent, independent, or linearly dependent on Λ. Interestingly, the two "present" energies agree on the definition of bending energy.

We will derive expansions to quadratic order in strain ε and thickness $z\partial_x\theta \leq t\partial_x\theta$, dropping any pure or mixed terms of higher order. Each expansion is different because the strains ε have different dependencies on stretch. All have the same structure at quadratic order in strain and thickness, namely a stretching term linear in thickness and quadratic in strain, and a bending term cubic in thickness and quadratic in a bending measure. Although it is a bit redundant, we write out each expansion to emphasize differences at higher order and in terms linear in thickness that, while integrating to zero for a symmetric plate, may be relevant in shells. The Green density is

$$\begin{aligned}
\mathcal{E}_{\text{Green}} &= \int_{-t/2}^{t/2} dz\, \tilde{Y} \left(\tfrac{1}{2}\left[(\Lambda - z\partial_x\theta)^2 - 1\right]\right)^2 \\
&= \int_{t/2}^{t/2} dz\, \tilde{Y} \left(\varepsilon_{\text{G}}^2 - 2z\varepsilon_{\text{G}}\Lambda\partial_x\theta + z^2\left(\Lambda\partial_x\theta\right)^2\right) + O\left(\text{cubic}\right) \\
&\approx t\tilde{Y}\left[\tfrac{1}{2}(\Lambda^2 - 1)\right]^2 + \tfrac{1}{12}t^3\tilde{Y}\left(\Lambda\partial_x\theta\right)^2 .
\end{aligned} \tag{2.16}$$

The Almansi density is

$$\begin{aligned}
\mathcal{E}_{\text{Almansi}} &= \int_{-t/2}^{t/2} dz\, \tilde{Y} \left(\tfrac{1}{2}\left[1 - \frac{1}{(\Lambda - z\partial_x\theta)^2}\right]\right)^2 , \\
&= \int_{-t/2}^{t/2} dz\, \tilde{Y} \left(\varepsilon_{\text{A}}^2 - 2z\varepsilon_{\text{A}}\partial_x\theta/\Lambda + z^2\left(\partial_x\theta/\Lambda\right)^2\right) + O\left(\text{cubic}\right) \\
&\approx t\tilde{Y}\left[\tfrac{1}{2}\left(1 - 1/\Lambda^2\right)\right]^2 + \tfrac{1}{12}t^3\tilde{Y}\left(\partial_x\theta/\Lambda\right)^2 .
\end{aligned} \tag{2.17}$$

The Biot density is special in that, given the prior assumptions in the approach we've taken,

it is exact at quadratic order,

$$\begin{aligned}\mathcal{E}_{\text{Biot}} &= \int_{-t/2}^{t/2} dz\, \tilde{Y} \left(\Lambda - z\partial_x\theta - 1\right)^2 \\ &= \int_{-t/2}^{t/2} dz\, \tilde{Y} \left(\varepsilon_{\text{B}}^2 - 2z\varepsilon_{\text{B}}\partial_x\theta + z^2(\partial_x\theta)^2\right) \\ &= t\tilde{Y}\left(\Lambda - 1\right)^2 + \tfrac{1}{12}t^3\tilde{Y}\left(\partial_x\theta\right)^2 . \end{aligned} \tag{2.18}$$

The Swainger density is

$$\begin{aligned}\mathcal{E}_{\text{Swainger}} &= \int_{-t/2}^{t/2} dz\, \tilde{Y} \left(1 - \frac{1}{\Lambda - z\partial_x\theta}\right)^2 \\ &= \int_{-t/2}^{t/2} dz\, \tilde{Y} \left(\varepsilon_{\text{S}}^2 - 2z\varepsilon_{\text{S}}\partial_x\theta/\Lambda + z^2\left(\partial_x\theta/\Lambda\right)^2\right) + O\left(\text{cubic}\right) \\ &\approx t\tilde{Y}\left(1 - 1/\Lambda\right)^2 + \tfrac{1}{12}t^3\tilde{Y}\left(\partial_x\theta/\Lambda\right)^2 . \end{aligned} \tag{2.19}$$

In this simple context, one can see upon close inspection that the non-Biot bending terms could be rewritten as Biot plus a higher-order correction. This clumsy additional step would be less apparent in a general treatment that does not admit a simple description in terms of a single stretch and angle.

2.4 Two simple deformations

Here we demonstrate the individual and combined behavior of the stretching and bending terms $\mathcal{E}_S$ and $\mathcal{E}_B$ from the four energies (2.16-2.19). The expansion of a closed circular ring and the extension of a circular arc at fixed radius will be considered.

The stretching contents of the four energies for a general deformation are shown in Figure 2.2. As is well known, the curves share a minimum, and thus are tangent to each other at $\Lambda = 1$, and remain close nearby. Important differences are found at large deformations, irrelevant to the present discussion of quadratic energies. The "reference" Green and Biot energies are bounded in compression ($\Lambda \to 0$) while the "present" Almansi and Swainger energies are bounded in tension ($\Lambda \to \infty$), reflecting the fact that the respective measures are normalized using reference or present quantities.

Consider a thin plate or beam, a body whose rest state is flat and of length L_0. The body is bent into a circular cylinder or ring, with its ends fused together (Figure 2.3). The resulting bending energies from the four models have qualitatively different dependencies on ring radius R. The material derivative of the angle, $\partial_x\theta$, and thus the Biot bending energy, are independent of radius. Expansion or contraction of a ring is "pure stretching" in the

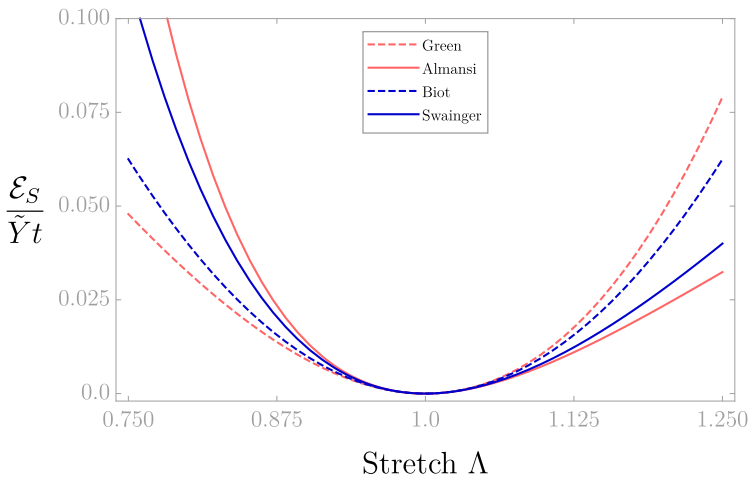

Figure 2.2: Stretching energy density $\mathcal{E}_S$ as a function of mid-line stretch Λ. Green and Biot are bounded as $\Lambda \to 0$ while Almansi and Swainger are bounded as $\Lambda \to \infty$.

Biot model, a definition preferred by Antman [33]. The identical Almansi and Swainger bending energies are given by the curvature, so decrease with increasing radius, approaching zero as the radius tends to infinity. The Green bending energy does the opposite — it approaches zero with the radius, and increases without bound as the ring expands and its curvature vanishes. These qualitative differences in bending energy appear as zero, negative, or positive slopes at unit stretch, when the mid-line strain vanishes. The curves are nowhere tangent to each other.

Consider the same plate bent into a circular arc of unit radius, and the dependence of the bending energies on the length of this arc or, equivalently, its subtended angle ϕ (Figure 2.4). The curvature, and thus the identical Almansi and Swainger bending energies, are independent of the subtended angle, making extension or compression of any arc at fixed radius "pure stretching" in either of these models. The Biot and Green bending energies increase without bound with subtended angle, and approach zero as the arc shortens to zero length.

What is "pure stretching" in the Green model? This would be any combination of changes in length and curvature that preserve the value of $\Lambda\partial_x\theta = \Lambda^2\partial_s\theta$. In terms of circular arcs, this could be achieved by simultaneous radial expansion and axial compression, or radial shrinkage and axial extension.

Returning to the closed ring of Figure 2.3a, the competition between stretching and bending may be seen in the total energies of Figure 2.5, calculated for a mid-line isometric radius of unity and a thickness $t = 0.05$. Among the class of symmetric circular solutions, only the Biot energy predicts a mid-line isometry as the ground state. Almansi and Swainger, which are close enough to be indistinguishable in the small stretch range of the figure, relieve bending energy through an expansion of the ring to a larger radius, while Green contracts

the ring. These shifts in the equilibrium stretch scale as the ratio of bending to stretching moduli, $t^2/12$, with corresponding decreases in the energy scaling as the square of this ratio. Explicitly, the minima are located at $\Lambda = (1 - t^2/6)^{1/2}$ for Green, $\Lambda = (1 - t^2/6)^{-1/2}$ for Almansi, $\Lambda = 1$ for Biot, and $\Lambda = 1 + t^2/12$ for Swainger.

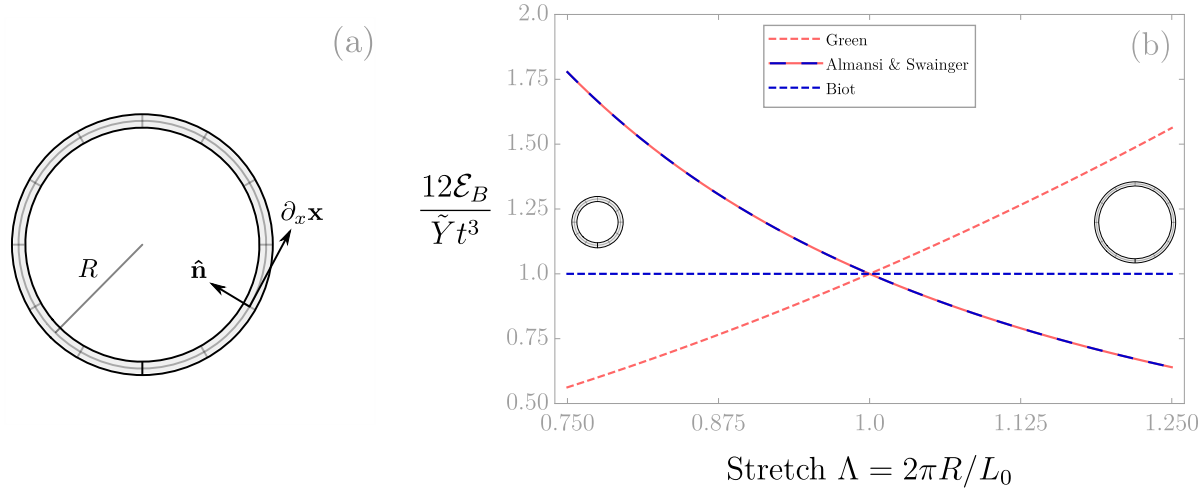

Figure 2.3: (a) Geometry of a closed ring of naturally flat material. (b) Bending energy densities as a function of ring radius R. Biot is independent of R and thus stretch Λ in this geometry. Green $\to 0$ as $R \to 0$ while Almansi/Swainger $\to 0$ as $R \to \infty$.

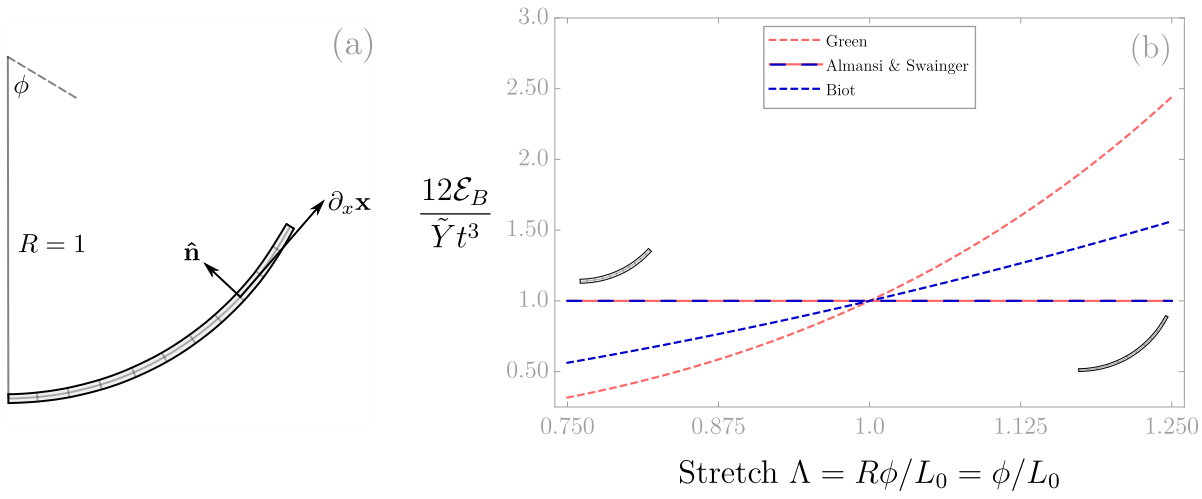

Figure 2.4: (a) Geometry of an open arc of naturally flat material. (b) Bending energy densities as a function of subtended angle ϕ. Almansi/Swainger is independent of ϕ and thus stretch Λ in this geometry. Green and Biot $\to 0$ as $\phi \to 0$.

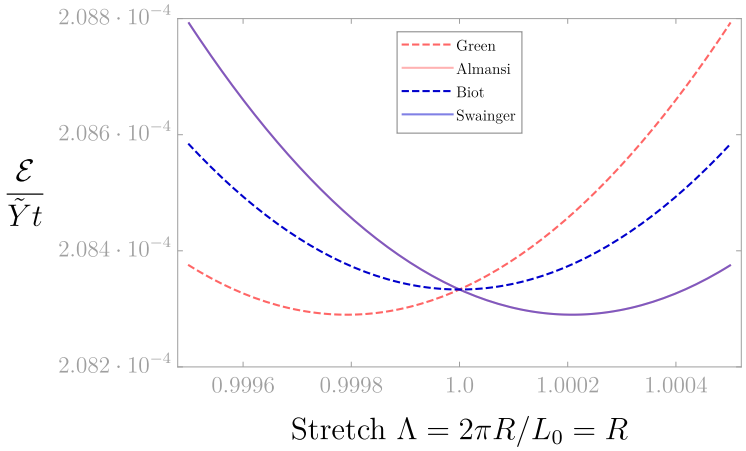

Figure 2.5: Total energy densities $\mathcal{E}$ as a function of ring radius R for the closed ring of Figure 2.3a with thickness $t = 0.05$ and $L_0 = 2\pi$. The difference between Almansi and Swainger energies is not visible in this range. These and Green experience shifts from the equilibrium Biot stretch of order $t^2/12$.

2.5 Concluding discussion

The Biot-Antman definition of pure stretching is that which remembers and respects the original symmetry of the plate. Changing the radius of a section of a bent, naturally flat body, while preserving its subtended angle, changes the lengths on either side of the mid-line by the same amount. A suitable modification of this definition should be possible for naturally curved bodies. Extension of our brief calculation to naturally curved beams and shells will likely prove informative.

All four quadratic energies have the same definition of pure bending, a change at constant stretch Λ in the kinematic variable $\partial_x\theta$, the material derivative of the angle. But only the Biot bending energy is simply the square of this variable, which should not be confused with the invariant curvature $\partial_x\theta/\Lambda$. The other energies could, however, be rewritten as Biot plus a small correction.

Our simple example of a closed ring of naturally flat plate material illustrates important differences between the limits of vanishing strain (mid-surface isometry) and vanishing thickness. The effects we have noted vanish with thickness, not with strain. At finite thickness, there are nontrivial effects of the choice of bending energy near isometry. In particular, only the Biot strain predicts an axisymmetric isometric ring as the ground state, despite the absence of any incompatibility between the mid-line metric and the boundary conditions. This is an important point, given that a primary interest in soft matter elasticity is the manner in which (self-)incompatibility of two-dimensional metrics causes stretching and bending of sheets. Additionally, those who seek to rationalize the behavior of soft plates and shells of finite thickness by invoking the concept of isometry might find a Biot model more agreeable

than the commonly employed Green model. Finally, the simplicity of expression (2.7) and exactness of the derivation (2.18) points to the possible role of stretch as a fundamental quantity, with its deviation from unity being the appropriate choice for expansions, rather than more complex fields such as the metrics that appear in Green and Almansi.

Thus we should reemphasize the potential value of a fully general Biot theory whose development was not required by the present simple example. Within the soft matter literature, Oshri and Diamant have recently developed an axisymmetric Biot theory [15], and Knoche and Kierfeld [24] have worked with Biot-like measures of bending in shells. A Biot theory would also connect with common bead-spring models [23]. The main hindrance appears to be the present lack of a simple and physics-friendly representation of a Biot energy in terms of position derivatives in arbitrary coordinates. An incompatible model would also require the concept of a reference stretch tensor akin to the reference metric employed in [1].

Bibliography

[1] E. Efrati, E. Sharon, and R. Kupferman. Elastic theory of unconstrained non-Euclidean plates. *Journal of the Mechanics and Physics of Solids*, 57:762–775, 2009.

[2] J.-H. Na, N. P. Bende, J. Bae, C. D. Santangelo, and R. C. Hayward. Grayscale gel lithography for programmed buckling of non-Euclidean hydrogel plates. *Soft Matter*, 12:4985–4990, 2016.

[3] J. Geng and J. V. Selinger. Deformation of an asymmetric thin film. *Physical Review E*, 86:036602, 2012.

[4] T.-S. Nguyen and J. V. Selinger. Theory of liquid crystal elastomers and polymer networks. *The European Physical Journal E*, 40:76, 2017.

[5] M. Pezzulla, N. Stoop, X. Jiang, and D. P. Holmes. Morphing of geometric composites *via* residual swelling. *Soft Matter*, 11:5812–5820, 2015.

[6] M. Marder and N. Papanicolaou. Geometry and elasticity of strips and flowers. *Journal of Statistical Physics*, 125(5/6):1069–1096, 2006.

[7] C. D. Santangelo. Buckling thin disks and ribbons with non-Euclidean metrics. *EPL*, 86:34003, 2009.

[8] J. Gemmer and S. C. Venkataramani. Shape transitions in hyperbolic non-Euclidean plates. *Soft Matter*, 9:8151, 2013.

[9] M. A. Dias, J. A. Hanna, and C. D. Santangelo. Programmed buckling by controlled lateral swelling in a thin elastic sheet. *Physical Review E*, 84:036603, 2011.

[10] C. D. Modes, K. Bhattacharya, and M. Warner. Gaussian curvature from flat elastica sheets. *Proceedings of the Royal Society A*, 467:1121–1140, 2011.

[11] P. Plucinsky, B. A. Kowalski, T. J. White, and K. Bhattacharya. Patterning nonisometric origami in nematic elastomer sheets. *Soft Matter*, 14:3127–3134, 2018.

[12] H. Aharoni, Y. Xia, X. Zhang, R. D. Kamien, and S. Yang. Universal inverse design of surfaces with thin nematic elastomer sheets. *PNAS*, 115(28):7206–7211, 2018.

[13] B. Audoly and A. Boudaoud. Self-similar structures near boundaries in strained systems. *Physical Review Letters*, 91:086105, 2003.

[14] E. Sharon, B. Roman, and H. L. Swinney. Geometrically driven wrinkling observed in free plastic sheets and leaves. *Physical Review E*, 75:046211, 2007.

[15] O. Oshri and H. Diamant. Strain tensor selection and the elastic theory of incompatible thin sheets. *Physical Review E*, 95:053003, 2017.

[16] J. A. Hanna. Some observations on variational elasicity and its application to plates and membranes. `https://arxiv.org/abs/1807.06426`.

[17] R. C. Batra. Linear constitutive relations in isotropic finite elasticity. *Journal of Elasticity*, 51:243–245, 1998.

[18] R. C. Batra. Comparison of results from four linear constitutive relations in isotropic finite elasticity. *International Journal of Non-Linear Mechanics*, 36:421–432, 2001.

[19] D. J. Steigmann. Two-dimensional models for the combined bending and stretching of plates and shells based on three-dimensional linear elasticity. *International Journal of Engineering Science*, 46:654–676, 2008.

[20] T. A. Witten. Stress focusing in elastic sheets. *Reviews of Modern Physics.*, 79:643–675, 2007.

[21] A. E. Green and W. Zerna. *Theoretical Elasticity*. Dover, Mineola, republication of second edition, 1992.

[22] O. Oshri and H. Diamant. Properties of compressible elastica from relativistic analogy. *Soft Matter*, 12:664–668, 2016.

[23] H. S. Seung and D. R. Nelson. Defects in flexible membranes with crystalline order. *Physical Review A*, 38(2):1005–1018, 1988.

[24] S. Knoche and J. Kierfeld. Buckling of spherical capsules. *Physical Review E*, 84:046608, 2011.

[25] T. Iwakuma and S. Kuranishi. How much contribution does the shear deformation have in a beam theory? *Structural Engineering/Earthquake Engineering, Proceedings of the Japan Society of Civil Engineers*, 344:141–151, 1984.

[26] T. Chaisomphob, F. Nishino, A. Hasegawa, and A. G. A. Abdel-Shafy. An elastic finite displacement analysis of plane beams with and without shear deformation. *Structural Engineering/Earthquake Engineering, Proceedings of the Japan Society of Civil Engineers*, 368:169–177, 1986.

[27] A. Magnusson, M. Ristinmaa, and C. Ljung. Behaviour of the extensible elastica solution. *International Journal of Solids and Structures*, 38:8441–8457, 2001.

[28] H. Irschik and J. Gerstmayr. A continuum mechanics based derivation of Reissner's large-displacement finite-strain beam theory: the case of plane deformations of originally straight Bernoulli-Euler beams. *Acta Mechanica*, 206:1–21, 2009.

[29] S. Antman. General solutions for plane extensible elasticae having nonlinear stress-strain laws. *Quarterly of Applied Mathematics*, 26(1):35–47, 1968.

[30] E. Reissner. On one-dimensional finite-strain beam theory: the plane problem. *ZAMP*, 23:795–804, 1972.

[31] A. B. Whitman and C. N. DeSilva. An exact solution in a nonlinear theory of rods. *Journal of Elasticity*, 4(4):265–280, 1974.

[32] P. A. Kelly. Mechanics Lecture Notes Part III: Foundations of Continuum Mechanics. `http://homepages.engineering.auckland.ac.nz/~pkel015/SolidMechanicsBooks/Part_III/`.

[33] S. S. Antman. *Nonlinear Problems of Elasticity*. Springer, New York, second edition, 2005.

Chapter 3

Swelling in anisotropic plates

The work presented in this chapter is part of a larger ongoing project on swelling in anisotropic plates. The contents of this chapter have not been published yet.

Attribution

The work presented in this chapter was done in collaboration with J. A. Hanna, who contributed to the inception and development of the main ideas in this work.

3.1 Introduction

The study of swelling gradients in thin plates and shells is one of great interest in the soft matter community. Several groups have explored the effects of through-thickness swelling gradients achieved via differential growth or shrinking between layers in isotropic elastic sheets [1, 2, 3, 4, 5]. In-plane swelling variations in isotropic elastic plates are also of interest [6], with [7] introducing a theoretical framework for the incompatible elasticity of plates and then applying said theory to a swollen hemispherical plate. Such studies provide valuable insight into the design of shape-programmable materials [8] and bistable morphing structures [9, 10].

The analysis of swelling gradients in plates and shells is not limited to isotropic materials. More recently, groups have studied swelling in nematic solids and liquid crystal elastomers [11, 12], which includes thin nematic elastomer strips that show transitions to twisted shapes [13, 14, 15]. Similar works have shown that swelling in anisotropic materials can aid in the design of three-dimensional printed structures [16, 17]. Outside of the soft matter community, studies have been conducted on composite materials widely used in the aerospace industry

[18, 19]. Studying swelling gradients in anisotropic materials can also be beneficial in the design of wooden architectural adaptive systems [20].

Inspired by warping in engineered wood products exposed to moisture, we look to study plates in which both the in-plane swelling and the material properties are anisotropic. We focus on plates loosely based on laminated veneer lumber, whose anisotropic stiffnesses lead to a separation of scales between individual bending energy terms. As early as the 1920's, the effects of moisture gradients during the construction and use of engineered wood products had been documented [21], with one of the first scientific studies on wood warp being conducted in 1940 [22]. Since then, work has been done on understanding the effects of moisture gradients in a wide variety of engineered wood products [23, 24, 25]. Theories and methods have been developed for the analysis of such systems, and existing theoretical plate models such as classical lamination theory have been applied to the wood warping problem [26].

Our work attempts to shed light on the unsolved problems of engineered wood warp by introducing a previously unused (in the context of the wood literature) incompatible elasticity model to predict warped shapes of anisotropic materials subject to anisotropic swelling. While the inception of this work is rooted in the wood industry, the treatment of the problem is general enough that it can be applied to a wide variety of anisotropic materials.

3.2 The system

As mentioned previously, the inspiration for this work comes from a common problem in the engineered wood product industry: flat panels warping out of plane due to differential swelling caused by moisture variation. Such a problem can be seen at multiple points during the lifespan of a wood panel: during the cooling phase after hot-pressing, while in storage, or during application. Our plate of interest is one that mimics the structure of an 8x4 foot laminated veneer lumber (LVL) panel. LVL consists of thin, rotary peeled wood veneers stacked, glued, and pressed together to form structurally sound panels designed to bear loads. Each veneer layer has a fiber direction with higher stiffness values and lower dimensional change coefficients when compared to the two transverse directions. LVL is stacked with all veneer fiber directions oriented parallel with the long dimension of the panel, so that the long direction is significantly stiffer than the others.

We model our anisotropic elastic plate as having lateral dimensions of $L = 2l$ and $W = l$ with thickness $h \ll l$. The fibers will be oriented with the long direction, see Figure 3.1. We use material coordinates x and y to denote the fiber and planar transverse to fiber directions, with the requirement that x be an arc length coordinate.

Swelling gradients of interest will vary with the x coordinate, and swelling will only occur in the planar transverse direction. Thus, the metric set by the swelling, or the programmed metric, will have the form $dx^2 + U(x)^2 dy^2$, where $U(x)^2$ is the swelling function specified by choosing $U(x)$. Corresponding to physical systems of interest, we will look at swelling

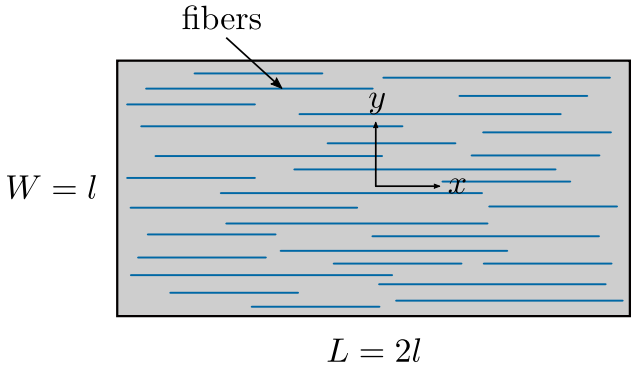

Figure 3.1: Schematic of anisotropic plate. Fibers are represented by thin, blue lines and are oriented in the long direction of the plate.

functions where the middle of the plate either shrinks or expands, relative to the outside.

To help guide our intuition when modeling these anisotropic plates, some simple physical models of plate warp were built. Models were constructed by cutting 8x4 inch sheets out of 0.005 inch thick plastic shim stock, with small slits 0.05 inches wide (at the widest point) cut out of the middle using a precision desktop cutter. The slits were oriented with the long direction of the plate to provide the necessary variation in swelling with the x coordinate. Thin, acrylic rods with a cross-sectional diameter of 0.0625 inches were glued down the length of the board in regular intervals to provide the anisotropic stiffness, see Figure 3.2. To simulate the middle of the plate shrinking, the slits were closed and held together with tape. For the middle expanding case the slits were opened further apart. As seen in Figure 3.3, the shapes were observed to be approximately cylindrical, with slight longitudinal curvature occurring near the very center of the plate where the swelling was at its greatest.

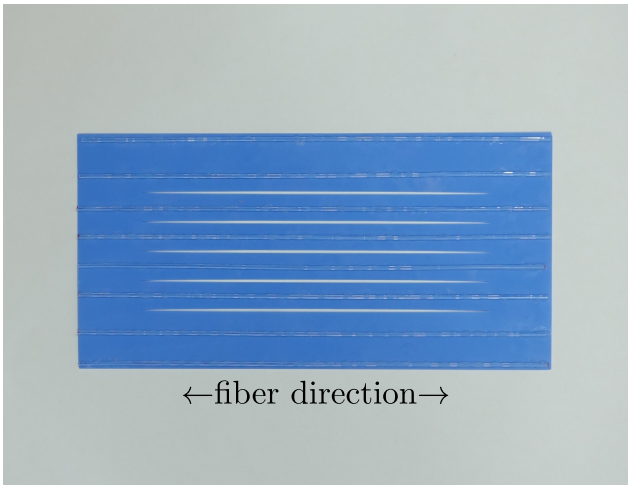

Figure 3.2: Top view of plate model before deformation. Clear acrylic rods line the lengthwise direction to provide the desired stiffness.

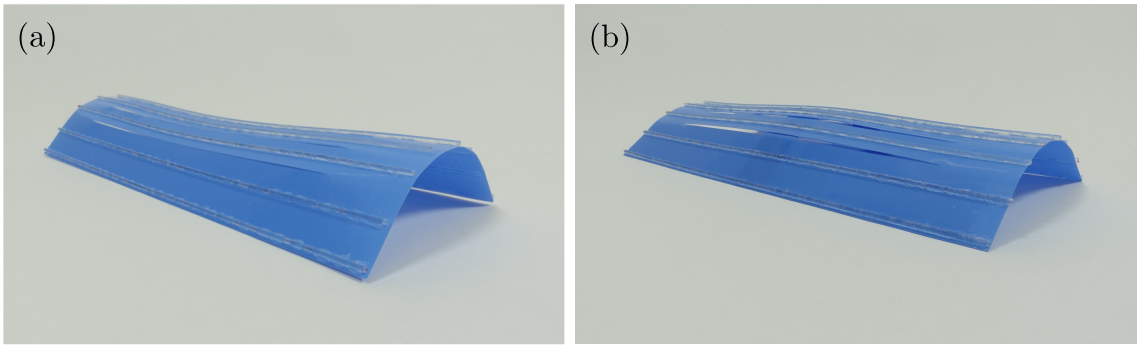

Figure 3.3: (a) Oblique view of plate model after slits were closed to simulate middle shrinking. (b) Oblique view of plate model after slits were opened further apart to simulate middle expanding.

Before any formal analysis is attempted, the resulting shapes of these models provide us with new information on anisotropic materials and swelling. As shown in [27], for a circular plate made from an isotropic material in which the isotropic swelling is greater in the middle of the plate, the resulting shape is a spherical dome with positive Gaussian curvature. Although our models are rectangular shaped and the swelling gradients are uni-directional, it is useful to make some comparisons between the two. Seen in Figure 3.3b, for an anisotropic material subject to the middle swelling there is a region similar to a spherical dome in the very middle of the plate, but closer to the ends the shape approximates a cylinder. Gaussian curvature is positive in the very middle, but changes sign and asymptotically approaches zero as one moves along the longitudinal direction towards the end of the plate. For an isotropic material where greater swelling occurs on the outer regions of a plate, the resulting shape is a saddle with negative Gaussian curvature [27]. Contrast this to Figure 3.3a, where there is a saddle-like region only in the middle, with cylindrical behavior becoming dominant towards the ends. For this model, Gaussian curvature starts negative in the middle, and as the longitudinal coordinate is increased, changes sign and approaches zero near the ends.

3.3 The energy

To write a general, covariant expression for the energy of an anisotropic plate in two dimensions, we start with the expression

$$E = \int dV \, \frac{1}{2} C^{ijkl} \epsilon_{ij} \epsilon_{kl},$$

where the indices take the range of the material coordinates x and y, C^{ijkl} are contravariant components of the elastic tensor, and ϵ_{ij} are covariant components of the strain tensor. (The

first Kirchhoff-Love assumption allows for the determination of the through-thickness strain as proportional to the in-plane strains through definition of appropriate material constants.) Following the standard procedures of a reduction from three to two dimensions [7], the strain ϵ_{ij} can be expressed as a function of the midsurface strain ε_{ij}, midsurface curvatures b_{ij}, and thickness coordinate z

$$E = \int dA \int_{-h/2}^{h/2} dz \, \frac{1}{2} C^{ijkl} (\varepsilon_{ij} - z b_{ij})(\varepsilon_{kl} - z b_{kl}) + O(\text{cubic}),$$

and upon integration through the thickness of the plate, we obtain an energy expression with a separation between the midsurface stretching and bending energies

$$E = \int dA \, \frac{1}{2} C^{ijkl} \left(h \varepsilon_{ij} \varepsilon_{kl} + \frac{h^3}{12} b_{ij} b_{kl} \right) + O(\text{cubic}). \tag{3.1}$$

In [28], a Cartesian representation of the elastic tensor for a transversely isotropic material is documented. We can take such an expression and apply it to our covariant, two dimensional formulation of an anisotropic material. For such a case, the elastic tensor takes the following form

$$\begin{aligned} C^{ijkl} = {} & \lambda g^{ij} g^{kl} + \mu_T \left(g^{ik} g^{jl} + g^{jk} g^{il} \right) + \alpha \left(q^k q^l g^{ij} + q^i q^j g^{kl} \right) \\ & + (\mu_L - \mu_T) \left(q^i q^k g^{jl} + q^i q^l g^{jk} + q^j q^k g^{il} + q^j q^l g^{ik} \right) + \beta q^i q^j q^k q^l, \end{aligned} \tag{3.2}$$

where λ, μ_T, μ_L, α, β are material constants related to the standard material constants (*i.e.* the elastic moduli, Poisson's ratios, and shear moduli), g^{ij} are contravariant components of the two dimensional surface metric, and q^i are contravariant components of the fiber direction unit vector.

For our purposes, we will constrain our surface such that it is an isometric deformation of the surface prescribed by the programmed metric, thus eliminating all stretching energy. Using (3.2) in (3.1) with the aforementioned constraint gives us

$$E = \int dA \, \frac{1}{2} \frac{h^3}{12} \left[\lambda b^i_i b^j_j + 2\mu_T b^i_j b^j_i + 2\alpha q^i q_j b^k_k b^j_i + 4(\mu_L - \mu_T) q^i q_j b^k_i b^j_k + \beta q^i q_j q^k q_l b^j_i b^l_k \right], \tag{3.3}$$

where we have dropped writing the existence of higher order terms. Further simplifications on (3.3) can be made in our case. As mentioned in the previous section, material coordinates x and y will denote the fiber and transverse directions, respectively. Thus, $q^x = q_x = 1$ and $q^y = q_y = 0$. We rename the elastic coefficients of (3.3) for simplicity $C_{(11)} = \lambda + 2\alpha + 4\mu_L - 2\mu_T + \beta$, $C_{(22)} = \lambda + 2\mu_T$, $C_{(12)} = \lambda + \alpha$, $C_{(66)} = \mu_L$, where the parentheses on the subscripts indicate that these are not tensorial objects, but rather coefficients. These coefficients are identical to the "reduced stiffnesses" in [18]. Thus, our bending energy takes the form

$$E = \iint \sqrt{g} \, dx dy \, \frac{1}{2} \frac{h^3}{12} \left[C_{(11)} (b^x_x)^2 + 4 C_{(66)} b^x_y b^y_x + 2 C_{(12)} b^x_x b^y_y + C_{(22)} (b^y_y)^2 \right], \tag{3.4}$$

where $dA = \sqrt{g} \, dx dy$ and g is the determinant of the metric.

3.4 The embedding

We are interested in studying cases where the swelling is anisotropic, only occurring in the y material coordinate direction and varying in the x material coordinate direction. Our metric programmed by the swelling will be of the form $dx^2 + U(x)^2 dy^2$, where $U(x)$ is a function of our choice.

We adopt a useful surface parameterization [29, 30] to embed these warped surfaces in three dimensional space, given by

$$\mathbf{x} = [\Lambda(x) + \chi\theta(x,y)]\,\hat{\mathbf{e}}_1 + \sqrt{\eta^2 U(x)^2 - \chi^2}\,[\cos\theta(x,y)\,\hat{\mathbf{e}}_2 + \sin\theta(x,y)\,\hat{\mathbf{e}}_3]\,, \tag{3.5}$$

where

$$\Lambda(x) = \int dx\, \frac{\eta U(x)}{\eta^2 U(x)^2 - \chi^2} \sqrt{\eta^2 U(x)^2\,(1 - \eta^2 U'(x)^2) - \chi^2},$$

and

$$\theta(x,y) = \frac{y}{\eta} - \frac{\chi}{\eta}\int dx\, \frac{\sqrt{\eta^2 U(x)^2\,(1 - \eta^2 U'(x)^2) - \chi^2}}{U(x)\,(\eta^2 U(x)^2 - \chi^2)}.$$

The surface is defined by a function $U(x)$ and two parameters η and χ, which control the "rolling up" and "twisting" of the surface, respectively. Such a surface is an ideal choice for this study, as its metric is of the same form as the programmed metric $dx^2 + U(x)^2 dy^2$, thus eliminating all stretching energy. In addition, we have a two parameter isometry with η and χ, allowing us to explore an isometric class of rolled and twisted shapes.

Curvatures for such an embedding are calculated with $b^i_j = g^{ik} b_{kj}$. Thus, the bending energy of the form (3.4) for a surface parameterized by (3.5) is

$$\begin{aligned} E = \iint U dx dy\, \frac{1}{2}\frac{h^3}{12} \Bigg[& C_{(11)} \left(\frac{\left(-\eta^4 U^3 U'' + \chi^2\right)^2}{\eta^4 U^4\,(\eta^2 U^2\,(1 - \eta^2 (U')^2) - \chi^2)} \right) + 4 C_{(66)} \left(\frac{\chi^2}{\eta^4 U^4} \right) \\ & - 2 C_{(12)} \left(\frac{U''}{U} - \frac{\chi^2}{\eta^4 U^4} \right) + C_{(22)} \left(\frac{1 - \eta^2\,(U')^2}{\eta^2 U^2} - \frac{\chi^2}{\eta^4 U^4} \right) \Bigg], \end{aligned} \tag{3.6}$$

where $\sqrt{g}\, dx dy = U dx dy$ is the volume form.

3.5 Results

Swelled shapes corresponding to energy minima are determined by selecting a function $U(x)$, numerically integrating (3.6) over dimensionless limits $-1 \le x/l \le 1$, $-1/2 \le y/l \le 1/2$, and minimizing the resulting expression with respect to η and χ.

To study middle shrinking and swelling, we choose a swelling function of the form $U(x) = 1 + a\,\mathrm{sech}(cx)$, where parameters a and c control the magnitude and the gradient of the

swelling, respectively. A positive value of a causes the middle of the plate to expand, while a negative value causes the middle to shrink.

For an example, we choose parameter values of $a = -0.05, 0.05$, $c = 4$ for $U(x)$, and choose material property values corresponding to yellow poplar LVL of $E_x = 14.3$, $E_y = 0.44$, $G_{xy} = 0.247$ GPa, $\nu_{xy} = 0.620$, $\nu_{yx} = 0.019$ from [31]. The reduced stiffnesses are calculated with $C_{(11)} = E_x/(1 - \nu_{xy}\nu_{yx}) = 14.471$, $C_{(22)} = E_y/(1 - \nu_{xy}\nu_{yx}) = 0.445$, $C_{(12)} = \nu_{xy}E_y/(1 - \nu_{xy}\nu_{yx}) = 0.276$, $C_{(66)} = G_{xy} = 0.247$ GPa. We then numerically minimize a dimensionless form of the energy

$$\frac{24E}{h^3 C_{(11)}} = \iint \sqrt{g}\, dxdy \left[(b_x^x)^2 + 4\frac{C_{(66)}}{C_{(11)}} b_y^x b_x^y + 2\frac{C_{(12)}}{C_{(11)}} b_x^x b_y^y + \frac{C_{(22)}}{C_{(11)}} (b_y^y)^2 \right], \tag{3.7}$$

with respect to η and χ. We find that for this example, the resulting shapes are axisymmetric with $\chi = 0$, see Figure 3.4.

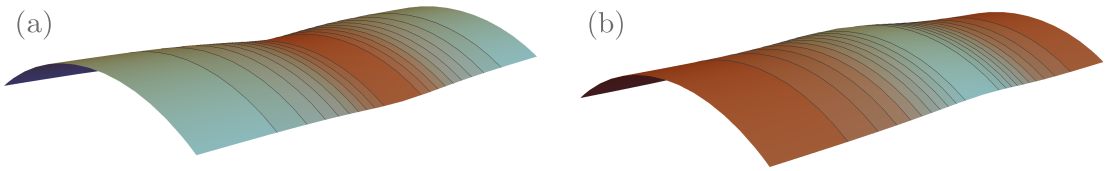

Figure 3.4: (a) Surface plot with swelling gradient for the middle shrinking case, with $a = -0.05$, $c = 4$, $\eta \approx 0.813$, $\chi = 0$. (b) Surface plot with swelling gradient for the middle expanding case, with $a = 0.05$, $c = 4$, $\eta \approx 0.789$, $\chi = 0$. Blue regions correspond to greater swelling.

For axisymmetric shapes, we can come up with a rough idea of how we should expect principal curvatures to scale with one another by minimizing the following bending energy expression $C_{(11)}(b_x^x)^2 + C_{(22)}(b_y^y)^2$ subject to a constraint on the Gaussian curvature using a Lagrange multiplier ζ. Minimizing the expression $C_{(11)}(b_x^x)^2 + C_{(22)}(b_y^y)^2 - \zeta(b_x^x b_y^y - K)$ with respect to the principal curvatures, we find that the principal curvatures should scale with $\left(\frac{b_x^x}{b_y^y}\right)^2 = \frac{C_{(22)}}{C_{(11)}}$. Figure 3.5 shows how well the scaling argument predicts the average squared ratio of curvatures for the example shrinking and expanding cases.

For swelling cases of the form $U(x) = 1 + a\,\mathrm{sech}(cx)$ where the middle shrinks, it is possible to tune both the swelling function parameters and the anisotropy of the material such that warped shapes become twisted, $\chi \neq 0$. As seen in Figure 3.6, decreasing the parameter c (effectively increasing the area of the panel that shrinks) results in a pitchfork bifurcation to a twisted solution. A similar pitchfork bifurcation is observed if we increase the value of a (increasing the magnitude of the shrinking) past a certain point (Figure 3.7). Figure 3.8 shows qualitative differences in the swelling function as the parameters a and c are varied. If we increase the stiffness of the material in the fiber direction, we see a bifurcation resembling

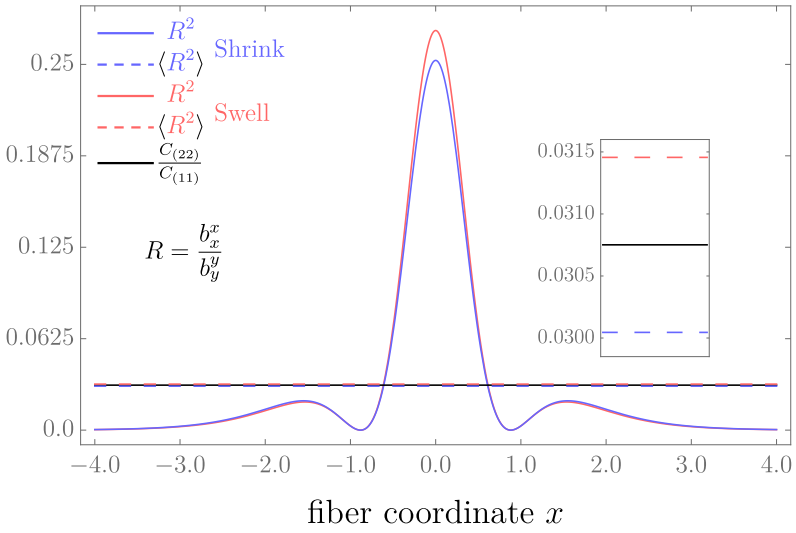

Figure 3.5: Squared ratio of curvatures $\left(\frac{b_x^x}{b_y^y}\right)^2$ plotted against the theoretical prediction $\frac{C_{(22)}}{C_{(11)}}$ for both middle shrink $a = -0.05$, $\eta \approx 0.813$, and middle swell $a = 0.05$, $\eta \approx 0.789$, with $c = 4$, $\chi = 0$.

that of a pitchfork, with χ growing with the fiber direction stiffness. As the stiffness is further increased, χ begins to slowly decrease (Figure 3.9). Further study into the nonlinear shape of this particular bifurcation could prove useful.

After studying the three parameters and their effects on twisted solutions for middle shrinking cases of the form $U(x) = 1 + a\,\mathrm{sech}(cx)$, we estimate that the parameter space would look something like what is shown in Figure 3.10. Little work has been done on investigating the same parameter space for cases where the middle expands, so we note that future work in this area would be valuable.

To study other twisted configurations, we choose the swelling function $U(x) = \sqrt{1 + (x/a)^2}$, where a is a parameter that controls the severity of the swelling. For an example where the middle shrinks, we choose $a = 5$ and numerically minimize the energy with respect to η and χ. We find that the resulting shape is completely twisted with $\eta = \chi = 5$; a section of the ruled surface known as the helicoid. For a material with one distinct stiff fiber direction, a ruled surface is a plausible equilibrium shape, as the bending energy term associated with the fiber direction can be completely eliminated by aligning the rulings of the surface with the fibers. In this case where the middle shrinks, the helicoid is selected as the resulting shape due to the longitudinal material coordinate lines needing to be closer together towards the middle of the plate. See Figure 3.11 for a visual demonstration of the helicoid.

For this form of swelling function, no matter the choice of a, the resulting shape will always be twisted with $\eta = \chi = a$, see Figure 3.12. Thus, with prior knowledge of the resulting

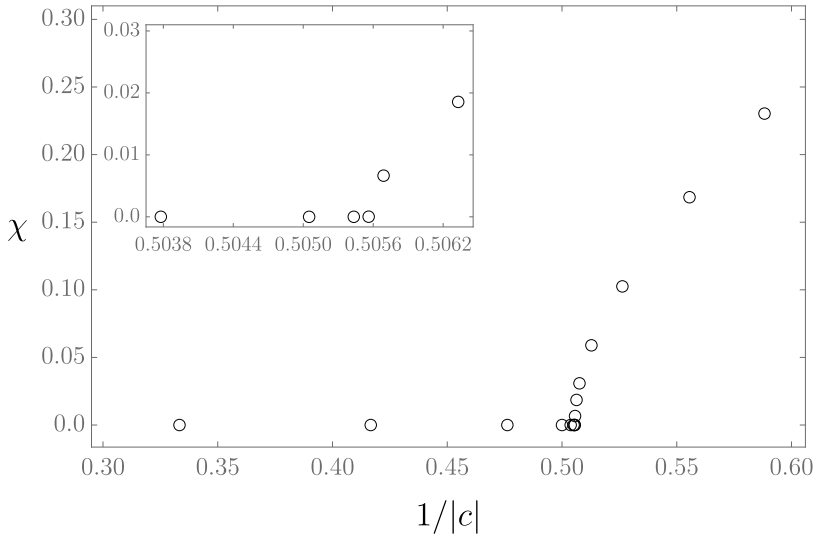

Figure 3.6: χ as a function of the parameter c for the case $U(x) = 1 + a\,\mathrm{sech}(cx)$, $a = -0.05$, with material property values of $C_{(11)} = 14.471$, $C_{(22)} = 0.445$, $C_{(12)} = 0.276$, $C_{(66)} = 0.247$ GPa.

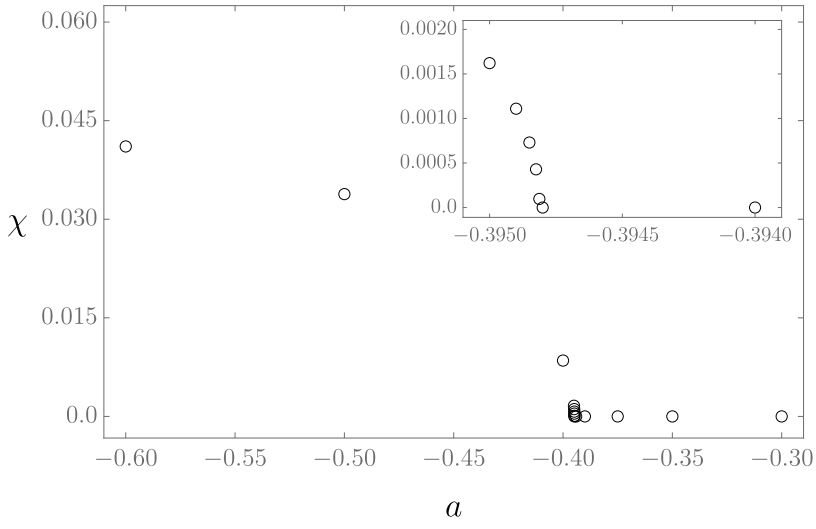

Figure 3.7: χ as a function of the parameter a for the case $U(x) = 1 + a\,\mathrm{sech}(cx)$, $c = 4$, with material property values of $C_{(11)} = 14.471$, $C_{(22)} = 0.445$, $C_{(12)} = 0.276$, $C_{(66)} = 0.247$ GPa.

shape we wish to study, if we set the value of $a = \eta$ the energy integral has an analytical

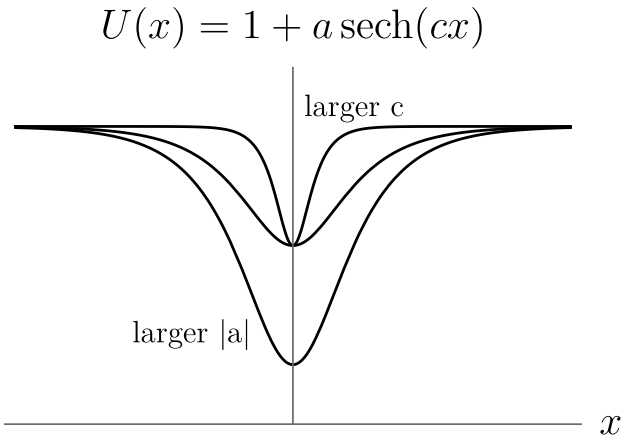

Figure 3.8: Qualitative plot of the middle shrinking case $U(x) = 1 + a\,\mathrm{sech}(cx)$ with parameters a and c varied. A larger value of c results in a more localized region of shrinking, and a larger value of a results in a larger amount of shrinking.

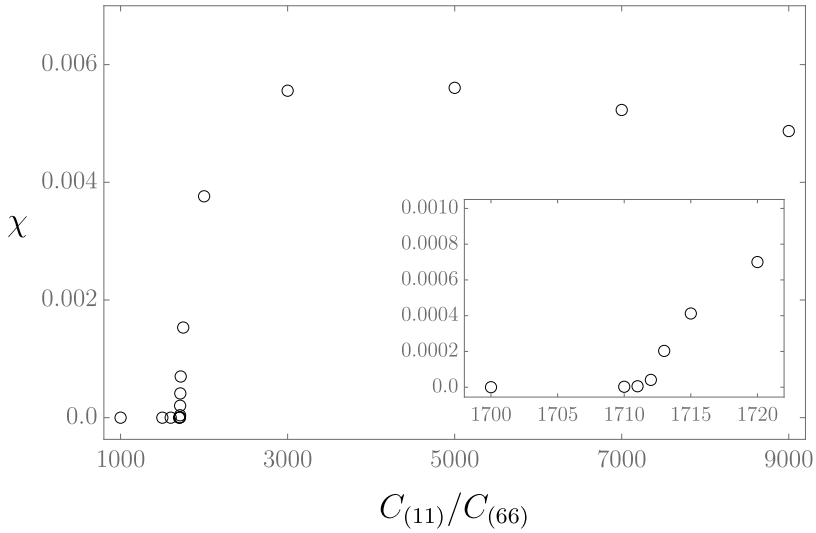

Figure 3.9: χ as a function of the material coefficient $C_{(11)}$ for the case $U(x) = 1 + a\,\mathrm{sech}(cx)$, $a = -0.05$, $c = 4$.

solution given by

$$\frac{24E}{h^3 C_{(11)}} = \frac{2}{\eta^3\sqrt{\eta^2+1}}\left(\eta^2\left(1 - 2\frac{C_{(12)}}{C_{(11)}} + \frac{C_{(22)}}{C_{(11)}}\right) - \chi^2\left(1 - 2\frac{C_{(12)}}{C_{(11)}} + \frac{C_{(22)}}{C_{(11)}} - 4\frac{C_{(66)}}{C_{(11)}}\right)\right).$$

For this example $0 \le \chi \le \eta$, thus the minimum of this expression occurs at $\chi = \eta$. For isotropic materials, $C_{(11)} = C_{(22)} = \nu C_{(12)} = Y/(1-\nu^2)$, $C_{(66)} = Y/(2(1+\nu))$, where Y is

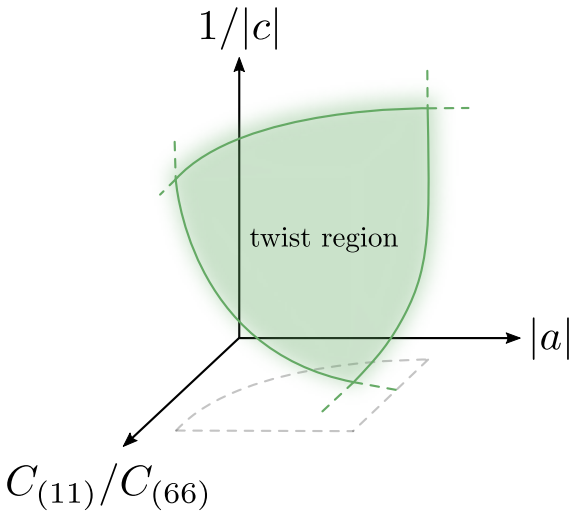

Figure 3.10: Qualitative sketch of the three parameter space for the middle shrinking case $U(x) = 1 + a\,\mathrm{sech}(cx)$. Solutions where twisting occurs are highlighted by the green area.

the elastic modulus and ν is Poisson's ratio, and the exact energy expression reduces to

$$\frac{24(1-\nu^2)E}{h^3 Y} = \frac{4(1-\nu)}{\eta^2\sqrt{\eta^2+1}},$$

which is independent of χ, demonstrating that such materials have a "soft mode" with respect to the twisting parameter. We have just shown that when the material is anisotropic, no such mode exists, and that a twisted embedding will be favored.

To understand why some choices of swelling functions result in axisymmetric shapes and others in twisted shapes, we look at each individual bending energy term in (3.6). For the $(b_y^y)^2$, $b_x^x b_y^y$, and $b_y^x b_x^y$ terms, it is clear how each behaves when χ is increased. Both $b_x^x b_y^y$ and $b_y^x b_x^y$ will increase with increasing χ, and $(b_y^y)^2$ will decrease with increasing χ. To determine how the dominant $(b_x^x)^2$ term behaves, we Taylor expand this term for small χ. Up to quadratic order in χ, we have

$$(b_x^x)^2 \approx \frac{\eta^2(U'')^2}{1-\eta^2(U')^2} + \left[\left(\frac{U''}{U(\eta^2(U')^2-1)}\right)^2 + \frac{2U''}{\eta^2U^3(\eta^2(U')^2-1)}\right]\chi^2 + O(\chi^4).$$

For physically immersible surfaces, $U > 0$, $\eta^2U^2 < 1$. Upon inspection of the twisting term in brackets, we notice that the first term is always positive, and that the denominator of the second term, $\eta^2U^3(\eta^2(U')^2 - 1)$, is always negative. Locally, the sign of U'' determines the overall sign of the twisting term. So for the twisting term to lower the overall value of the $(b_x^x)^2$ term, U'' needs to be positive and large enough for a sufficiently large region over the plate domain.

This argument is applicable in the limit of large anisotropy $C_{(11)} \to \infty$. As $C_{(11)} \to \infty$, the first term in (3.7) becomes dominant as the other terms approach zero. Thus for small χ,

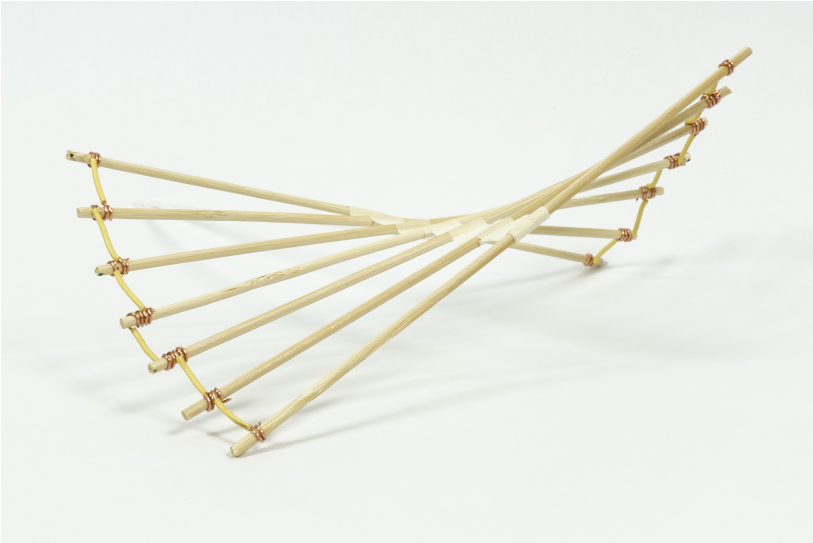

Figure 3.11: Oblique view of helicoid surface model. Rulings are represented by the thin, wooden rods. Transverse distance between rulings is greater at the ends held together by wire than in the middle, which has been pinched together with tape.

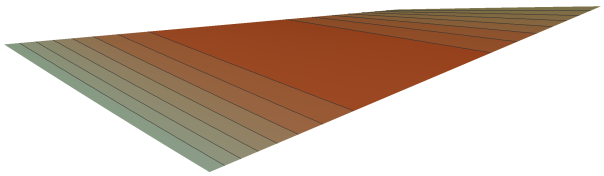

Figure 3.12: Surface plot with swelling function for the completely twisted case of $U(x) = \sqrt{1+(x/a)^2}$, $a = 5$, $\eta = 5$, $\chi = 5$. Blue regions correspond to greater swelling.

the $O(\chi^2)$ in the Taylor expansion of $(b_x^x)^2$ will determine if twisting increases or decreases the total energy. For moderately anisotropic materials, every term must be taken into consideration, and the analysis becomes more complicated. For swelling functions of the form $U(x) = 1 + a\,\mathrm{sech}(cx)$ where twisted shapes are observed, the existence of twisting is allowing for the relaxation of longitudinal and transverse bending energy for some added twisting energy. Due to the relative magnitudes of the material stiffnesses, this twisting lowers the total energy.

Bibliography

[1] N. A. Caruso, A. Cvetković, A. Lucantonio, G. Noselli, and A. DeSimone. Spontaneous morphing of equibiaxially pre-stretched eastic bilayers: the role of sample geometry. *International Journal of Mechanical Sciences*, 000:1–6, 2017.

[2] M. Pezzulla, G. P. Smith, P. Nardinocchi, and D. P. Holmes. Geometry and mechanics of thin growing bilayers. *Soft Matter*, 12:4435–4442, 2016.

[3] J. Geng and J. V. Selinger. Deformation of an asymmetric thin film. *Physical Review E*, 86:036602, 2012.

[4] D. P. Holmes, M. Roché, T. Sinha, and H. A. Stone. Bending and twisting of soft materials by non-homogeneous swelling. *Soft Matter*, 7:5188–5193, 2011.

[5] W. M. van Rees, E. Vouga, and L. Mahadevan. Growth patterns for shape-shifting elastic bilayers. *PNAS*, 114:11597–11602, 2017.

[6] J. Kim, J. A. Hanna, R. C. Hayward, and C. D. Santangelo. Thermally responsive rolling of thin gel strips with discrete variations in swelling. *Soft Matter*, 8:2375–2381, 2012.

[7] E. Efrati, E. Sharon, and R. Kupferman. Elastic theory of unconstrained non-Euclidean plates. *Journal of the Mechanics and Physics of Solids*, 57:762–775, 2009.

[8] M. A. Dias, J. A. Hanna, and C. D. Santangelo. Programmed buckling by controlled lateral swelling in a thin elastic sheet. *Physical Review E*, 84:036603, 2011.

[9] Z. Chen, Q. Guo, C. Majidi, W. Chen, D. J. Srolovitz, and M. P. Haataja. Nonlinear geometric effects in mechanical bistable morphing structures. *Physical Review Letters*, 109:114302, 2012.

[10] S. Daynes, C. G. Diaconu, K. D. Potter, and P. M. Weaver. Bistable prestressed symmetric laminates. *Journal of Composite Materials*, 44:1119–1137, 2010.

[11] B. A. Kowalski, C. Mostajeran, N. P. Godman, M. Warner, and T. J. White. Curvature by design and on demand in liquid crystal elastomers. *Physical Review E*, 97:012504, 2018.

[12] H. Aharoni, Y. Xia, X. Zhang, R. D. Kamien, and S. Yang. Universal inverse design of surfaces with thin nematic elastomer sheets. *PNAS*, 115(28):7206–7211, 2018.

[13] L. Teresi and V. Varano. Modeling helicoid to spiral-ribbon transitions of twist-nematic elastomers. *Soft Matter*, 9:3081–3088, 2013.

[14] G. Tomassetti and V. Varano. Capturing the helical to spiral transitions in thin ribbons of nematic elastomers. *Meccanica*, 52:3431–3441, 2017.

[15] Y. Sawa, F. Ye, K. Urayama, T. Takigawa, V. GiminezPinto, R. L. B. Selinger, and J. V. Selinger. Shape selection of twist-nematic-elastomer ribbons. *PNAS*, 108:6364–6368, 2011.

[16] A. S. Gladman, E. A. Matsumoto, R. G. Nuzzo, L. Mahadevan, and J. A. Lewis. Biomimetic 4D printing. *Nature Materials*, 15:413–419, 2016.

[17] D. C. Zuluaga and A. Menges. 3D printed hygroscopic programmable material systems. *Materials Resources Society Symposium Proceedings*, 1800:1–8, 2015.

[18] M. W. Hyer. Calculations of the room-temperature shapes of unsymmetric laminates. *Journal of Composite Materials*, 15:296–310, 1981.

[19] J. Steeves and S. Pellegrino. Post-cure shape error of ultra-thin symmetric CFRP laminates: Effect of ply-level imperfections. *Composite structures*, 164:237–247, 2017.

[20] S. Abdelmohsen, S. Adriaenssens, R. El-Dabaa, and S. Gabriele. A multi-physics approach for modeling hygroscopic behavior in wood low-tech architectural adaptive systems. *Computer-Aided Design*, 106:43–53, 2019.

[21] B. C. Boulton. *The Manufacture and Use of Plywood and Glue*. Sir Isaac Pitman & Sons, LTD., Parker Street, Kingsway, W.C., 1920.

[22] D. Brouse. Some causes of warping in plywood and veneered products. Forest Products Laboratory Report No. 1252:1–10, 1961.

[23] B. G. Heebink, E. W. Kuenzi, A. C. Maki, and C. B. Norris. Linear movement of plywood and flakeboards as related to the longitudinal movement of wood. Forest Products Laboratory Report No. 073:1–33, 1964.

[24] O. Suchsland and J. D. McNatt. Computer simulation of laminated wood panel warping. *Forest Products Journal*, 36:16–23, 1986.

[25] E. M. Lang, J. R. Loferski, and J. D. Dolan. Hygroscopic deformation of wood-based composite panels. *Forest Products Journal*, 45:67–70, 1995.

[26] Z. Cai and J. R. Dickens. Wood composite warping: modeling and simulation. *Wood and Fiber Science*, 36:174–185, 2004.

[27] Y. Klein, E. Efrati, and E. Sharon. Shaping of elastic sheets by prescription of non-Euclidean metrics. *Science*, 315:1116–1120, 2007.

[28] A. J. M. Spencer. *Continuum Theory of the Mechanics of Fibre-Reinforced Composites*. Springer Verlag, New York, 1984.

[29] K. Kenmotsu. *Surfaces with Constant Mean Curvature*. American Mathematical Society, Providence, Rhode Island, 2003.

[30] M. P. do Carmo and M. Dajczer. Helicoidal surfaces with constant mean curvature. *Tôhoku Mathematical Journal*, 34:425–435, 1982.

[31] J. J. Janowiak, D. P. Hindman, and H. B. Manbeck. Orthotropic behavior of lumber composite materials. *Wood and Fiber Science*, 33:580–594, 2001.